

# Novel x-ray diffractometer for liquid surface studies

A. H. Weiss,<sup>a)</sup> M. Deutsch,<sup>b)</sup> A. Braslau, B. M. Ocko, and P. S. Pershan

*Division of Applied Sciences, Harvard University, Cambridge, Massachusetts 02138*

(Received 14 March 1986; accepted for publication 12 May 1986)

An x-ray diffractometer for studying the structure of the liquid-vapor interface is described. It is designed to permit reflectivity and scattering studies from liquid surfaces for angles varying from grazing incidence, below the critical angle for total external reflection up to angles  $\sim 3^\circ$  using a rotating anode x-ray generator. In principle the diffractometer system can be used to study both the density profile normal to the surface and in-plane structural features. The former is determined by deviations of the measured reflectivity from the Fresnel law of classical optics and the latter from nonspecular scattering. Results obtained using this spectrometer to measure the density profile normal to the surface of water and a liquid crystal are presented.

## INTRODUCTION

The density profile and in-plane structure of the liquid-vapor interface layer have attracted ever increasing research attention over the past decade.<sup>1-7</sup> The overwhelming majority of these studies were, however, either analytical,<sup>1,2,5-7</sup> or computer simulations.<sup>3,4,8</sup> Experiments were confined almost exclusively to macroscopic (surface tension,<sup>9</sup> viscoelastic properties,<sup>10,11</sup> etc.) or semimicroscopic (light scattering,<sup>12,13</sup> ellipsometry,<sup>14,15</sup> etc.) studies. Methods such as low-energy electron diffraction (LEED) and light atom or ion scattering, which prove to be useful experimental tools for studying the microscopic structure of solid surfaces, are almost completely excluded by the high vapor pressure of liquids. Furthermore, conventional x-ray methods, the microscopic structural tools *par excellence* for bulk studies, were rendered useless because of the relative weakness of the signal originating at the thin surface layer compared with scattering from the bulk. Although theoretical predictions of microscopic surface structure abound in fields of research as varied as superfluid helium,<sup>16-18</sup> liquids metals,<sup>19,20</sup> and liquid crystals,<sup>21</sup> relevant data was, until recently, virtually nonexistent. The only exceptions had been the recent work by Pershan and collaborators on liquid crystals<sup>22</sup> and the work on liquid mercury, cesium, and gallium carried out by Rice and co-workers<sup>23-25</sup> and Bosio *et al.*<sup>26,27</sup>

A method for probing the structure of liquid crystals and other liquids in the direction normal to the surface for use with a synchrotron radiation source was developed by one of us (PSP) and Als-Nielsen.<sup>22,28,29</sup> The density profile and other features of the surface layer are determined from the deviation of the measured reflectivity from the Fresnel reflection law. This method was first applied to liquid crystals<sup>29</sup> and, very recently, to water<sup>30</sup> and simple organic solvents.<sup>31</sup> A complimentary method employing out-of-reflection-plane diffraction under conditions of total external reflection was developed by Eisenberger and co-workers<sup>32,33</sup> for in-plane surface structure studies of solids and surface overlayers on solids. Recently, Bloch *et al.*<sup>34</sup> demonstrated the application to fluid surfaces of the method developed by Becker, Golovchenko, and Patel<sup>35</sup> for solids, by which x-ray fluorescence stimulated by x rays incident below the critical angle is used to interpret structure normal to the surface.

In this paper we describe a novel high-resolution surface diffractometer for use with a rotating anode x-ray generator. It can accommodate both solid and liquid samples, and in principle, provides for x-ray structure determinations both parallel and normal to the surface of the sample. X-ray reflectivity results are presented for the structure normal to the surface of water and a liquid crystal.

## I. DETAILS OF DESIGN

X-ray reflectivity measurements of a liquid surface impose several technical constraints on a spectrometer system. First, the scattering geometry must be arranged so that the liquid-gas interface remains normal to the earth's gravitational field, i.e., the sample cannot be tilted. Secondly, although the surface is nearly 100% reflecting for angles of incidence  $\alpha$  (defined in this paper with respect to the surface plane) less than the critical angle  $\alpha_c$ , the signal reflected from the surface decreases very rapidly with increasing angle,<sup>29,36</sup> i.e., for  $\alpha \gg \alpha_c$ , the reflectivity is  $\sim [\alpha_c / (2\alpha)]^4$ . For instance, the reflectivity of the surface of water for x-rays with  $\lambda = 1.54 \text{ \AA}$  is nearly 1 for  $\alpha$  less than  $\alpha_c \simeq 0.15^\circ$  but drops below  $10^{-6}$  at  $\alpha \simeq 2.4^\circ$ . At such small angles, finite sample size requires that the incident x-ray beam be both well collimated and spatially small. For example (taking the critical angle for water as a convenient reference value), at  $\alpha = 0.15^\circ$ , a 0.1-mm-high beam projects into a 40-mm-long x-ray illuminated footprint on the sample. In addition, the position of the sample relative to the beam must also be precisely controlled. Again taking  $\alpha = 0.15^\circ$  as an example, a 0.1-mm displacement of the sample in the vertical direction will cause the beam footprint to translate along the surface by 40 mm.

Further design considerations in this case were imposed by the fixed position of the source (a Rigaku RU-200 12-kW rotating anode x-ray generator) and the requirement of providing for both reflectivity and out-of-reflection-plane diffraction measurements. Because of the difference in characteristic collimation and wavelength distributions, the spectrometer designs that had been used in synchrotron studies of liquid surfaces are not optimal for use with the rotating anode source.

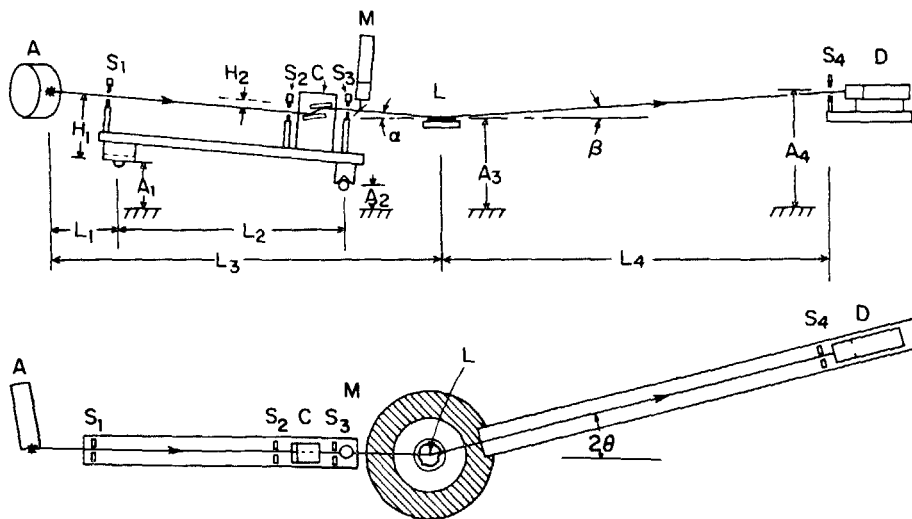


FIG. 1. (a) Schematic diagram of the x-ray diffractometer (side view). Slits  $S_1$ – $S_4$ ; A is the x-ray generator anode, C is the Ge[111] double bounce monochromator crystal, M is the beam monitor, L is the liquid sample, and D is the detector. (b) Schematic diagram of the x-ray diffractometer (top view). Slits  $S_1$ – $S_4$ ; A is the x-ray generator anode, C is the Ge[111] double bounce monochromator crystal, M is the beam monitor, L is the liquid sample, and D is the detector.

The design solution chosen for the rotating anode source is shown in Fig. 1. The spectrometer consists of four units: the monochromator arm which defines the incident beam, the horizontal two-circle goniometer,<sup>37</sup> the sample positioning stage, and the detector arm which defines the diffracted beam.

The monochromator arm consists of an aluminum U section to which three slits  $S_1$ ,  $S_2$ , and  $S_3$  are rigidly attached. The slits  $S_1$  and  $S_2$  define the incident beam direction and dimensions. These slits are followed by a Bonse–Hart-type<sup>38</sup> two-reflection channel cut germanium [111] monochromator mounted on a combined rotation-vertical translation unit. The slit  $S_3$  after the monochromator serves to reduce spurious scattering. The monochromator assembly is followed by an incident beam monitor consisting of a thin Kapton sheet which scatters about 0.1% of the incident beam into a scintillation detector. The monochromator arm is supported at each end on pivot supports ( $P_1$  and  $P_2$ ) mounted on independent elevators ( $E_1$  and  $E_2$ ). The liquid sample (L) is mounted on a third elevator ( $E_3$ ). X-rays reflected from the sample may be detected by a NaI(Tl) scintillation detector preceded by a slit ( $S_4$ ), mounted on the fourth elevator ( $E_4$ ) or by a position-sensitive proportional counter.<sup>22</sup> The sample and its elevator  $E_3$  are mounted on the inner ( $\phi$ ) circle of the horizontal two-circle goniometer. The slit-detector assembly along with its elevator  $E_4$  are mounted on a counter-weighted arm attached to the concentric, outer ( $2\theta$ ) circle of the horizontal goniometer. All four elevators<sup>39</sup> are positioned via stepping motors with a resolution of 0.4  $\mu\text{m}$  per step.

It is convenient to describe the geometry of a surface scattering experiment in terms of  $\lambda$ , the x-ray wavelength and four angles (see Fig. 2): (1)  $\alpha$ , the angle between the surface plane and wave vector  $\mathbf{k}_i$  of the incident ray; (2)  $\beta$ , the angle between the surface plane and the wavevector  $\mathbf{k}_o$  of the scattered ray; (3)  $2\theta$ , the angle between the projections of  $\mathbf{k}_i$  and  $\mathbf{k}_o$  onto the surface plane; and (4)  $\phi$ , the angle between the projection of  $\mathbf{k}_i$  into the surface plane and some preferred orientation in that plane such as a lattice vector, molecular tilt projection, etc.<sup>40</sup> The physics of the scattering experiment can often be described in terms of the wave-vec-

tor transfer  $\mathbf{q} = \mathbf{k}_o - \mathbf{k}_i$ . Expressions relating  $\mathbf{q}$  to the angles  $\alpha$ ,  $\beta$ ,  $2\theta$ , and  $\phi$  are given in Appendix B, while the method of setting the diffractometer to a given set of angles is detailed below.

Initial lineup (Appendix C) ensures that the beam centerline, as defined by  $S_1$  and  $S_2$ , is horizontal. The monochromator, which uses an even number of reflections, does not alter the beam direction. The angle of incidence  $\alpha$  is varied by tilting the monochromator arm as a whole without any adjustment of its individual elements. The tilt is defined by the positions of elevator  $E_1$  and  $E_2$  such that slits  $S_1$  and  $S_2$  track the fixed source. Intensity variations due to tracking errors are small. However, slight variations in the apparent source intensity can be corrected for using the beam monitor. The x-ray beam is rectangular in cross section with a horizontal width that is much greater than its height. Typical slit settings and the corresponding intensities are given in Table I.

The entire spectrometer is under computer control. For each setting of  $\alpha$ , the sample elevator height automatically moves to a position such that the incident beam centerline intercepts the surface at a fixed point on the sample. The

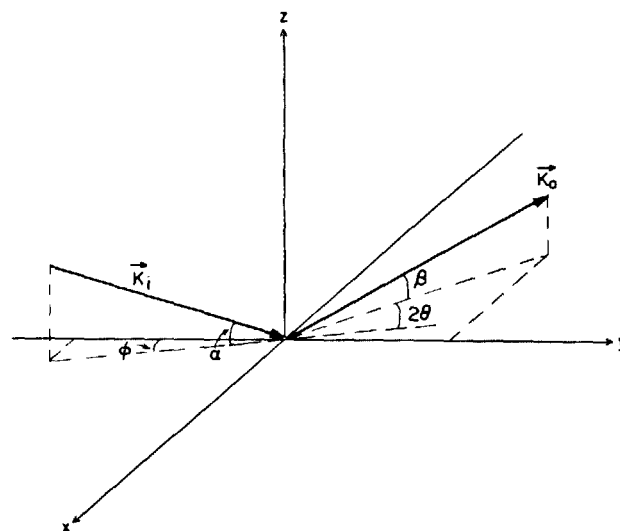


FIG. 2. Scattering geometry. See Appendix A for details.

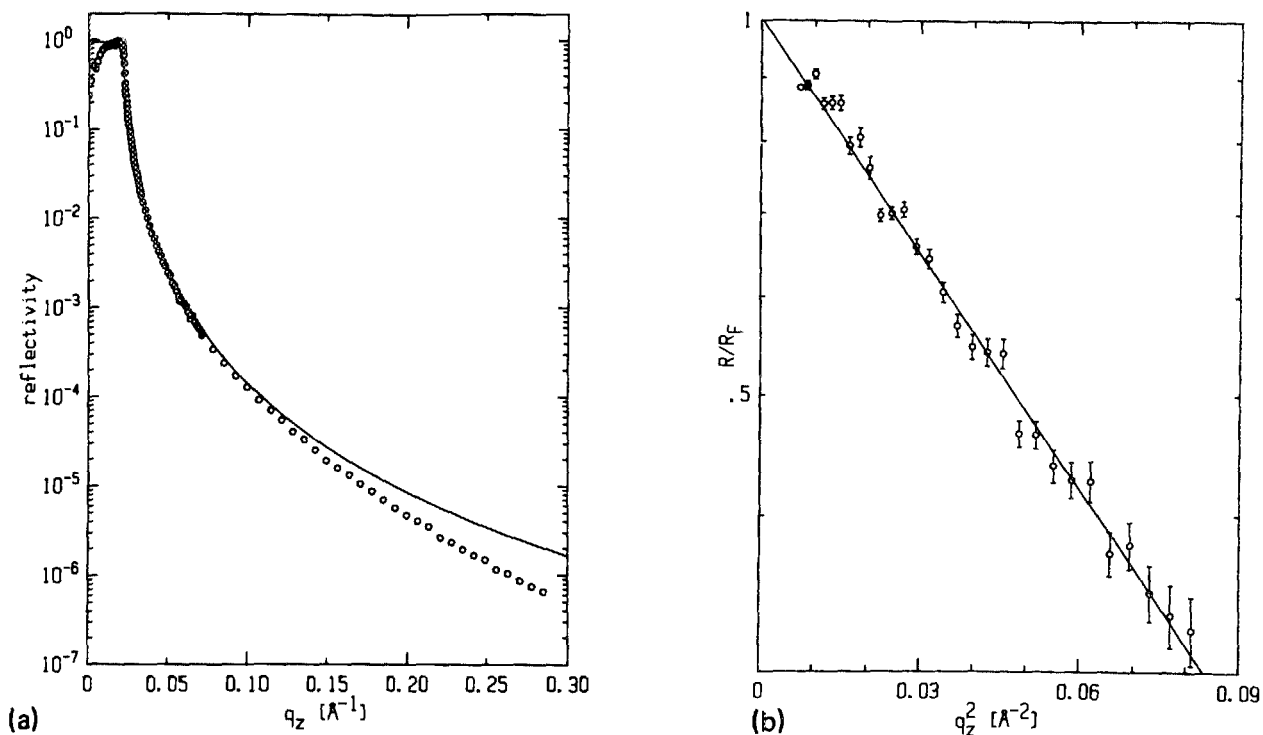


FIG. 3. (a) X-ray reflectivity of the surface of liquid water. The solid line is the Fresnel law of classical optics. (b) Ratio of the reflectivity of water to Eq. (2). A straight line fits the form  $|\phi|^2 = e^{-\langle u^2 \rangle q^2}$  with  $\langle u^2 \rangle = 3.8 \pm 0.03 \text{ \AA}$ .

angle  $\beta$  is fixed by setting the detector assembly at the required relative to the sample surface. This assembly consists of a single slit S4 and a scintillation detector. A more elaborate detection setup might utilize a linear detector or an analyzer crystal.

The angles  $\phi$  and  $2\theta$  are set simply by rotating the two concentric circles of the horizontal goniometer to the required values.

The two pivots  $P_1$  and  $P_2$  together constitute a kinematic support system for the monochromator arm. Pivot  $P_2$  is made up of a V block resting on a steel rod. The rod is mounted on an adjustable tilting stage which determines the tilt of the x-ray beam transverse to the direction of propagation. Pivot  $P_1$  is made up of a V block mounted at right angles to  $P_2$  and resting on a steel ball. This not only locates the arm to a fixed vertical plane, but also provides a sliding degree of

freedom which permits the horizontal distance between the two pivot points to remain constant as the monochromator arm is tilted.

The liquid samples are placed on a flat, polished glass surface. The glass flat and liquid are contained in a sealed, temperature-controlled sample chamber. The cell is mounted on a two-axis leveling stage attached to the elevator  $E_3$ . The elevator and sample assembly rests on a foam pad on the  $\phi$  circle of the horizontal goniometer. The foam, as well as a large lead mass, provides isolation from high-frequency vibrations.

The operation of the diffractometer, as well as data acquisition and display, are fully computerized using a Digital Equipment Corporation PDP 11/34a microcomputer with a CAMAC interface.

## II. EXPERIMENTAL RESULTS

For a perfectly flat surface with a step function discontinuity in the electron density, the x-ray reflectivity varies according to the Fresnel law,<sup>41</sup>  $R_F(\alpha)$ , where  $\alpha$  is the angle of incidence with respect to the surface. The refractive index of matter for x rays is less than unity by an amount  $\delta = \rho_e / \pi (e^2 / mc^2) \lambda^2 \sim 10^{-6}$ , where  $\rho_e$  is the electron density.<sup>41,42</sup> Therefore, total external reflection occurs at angles less than

$$\alpha_c = \cos^{-1}(n) \approx (1 - n^2)^{1/2} \approx [1 - (1 - \delta)^2]^{1/2} \approx (2\delta)^{1/2} \propto \rho^{1/2}. \quad (1)$$

This critical angle is of the order of a few tenths of a degree. For  $\alpha \ll 1$  but  $\alpha > \alpha_c$ , the Fresnel equations reduce to

TABLE I. Representative slit settings and intensities of the spectrometer.  $I_0$  and  $M_0$  are the incident and monitor intensities, respectively, for the Rigaku RU-200 rotating anode x-ray generator with a  $0.3 \times 0.3 \text{ mm}^2$  focused source operating at 4.5 kW.

	High resolution		Low resolution	
	Height (mm)	Width (mm)	Height (mm)	Width (mm)
$S_1$	0.100	1	0.4	4
$S_2$	0.075	1	0.3	4
$S_3$	1.	2	1	5
$S_4$	1.	5	1.5	14
$I_0$	$\sim 10^4$ counts/s		$\sim 3 \times 10^6$ counts/s	
$M_0$	$\sim 10$ counts/s		$\sim 3000$ counts/s	

$$R_F(\alpha) \approx \left| \frac{\alpha_c}{\alpha + (\alpha^2 - \alpha_c^2)^{1/2}} \right|^4 \approx \left( \frac{\alpha_c}{2\alpha} \right)^4, \quad (2)$$

when  $\alpha \gg \alpha_c$ . For a surface having an arbitrary density profile  $\rho(x, y, z)$ , one defines an average over the surface:

$$\langle \rho(z) \rangle = \frac{1}{A} \int \rho(x, y, z) dx dy, \quad (3)$$

where the  $z$  axis is normal to the surface. The reflectivity  $R(q)$  is modified<sup>22,28,30,31,43,44</sup> to give

$$R(q) = R_F(q) |\phi(q)|^2, \quad (4)$$

where for  $\alpha \gg \alpha_c$ ,

$$\phi(q) \approx \frac{1}{\langle \rho_0 \rangle} \int_{-\infty}^{\infty} \left\langle \frac{\partial \rho(z)}{\partial z} \right\rangle e^{-iqz} dz, \quad (5)$$

where

$$q = q_z = (4\pi/\lambda) \sin(\alpha), \quad (6)$$

and  $\langle \rho_0 \rangle$  is the average bulk density.

Using the formalism summarized above, it is possible to test models of the density profile and surface roughness against measured x-ray reflectivity curves. In the following paragraphs we present experimental reflectivity curves obtained for pure water and a liquid crystal and discuss the surface roughness and density profile of each inferred from this data.

Since mechanical vibrations induced macroscopically observed surface waves that made practical measurements impossible, it was necessary to use a thin enough water sample so that the long-wavelength, low-frequency waves were suppressed. The sample was prepared by spreading a 0.3-mm-thick layer of water on a 78-mm-diam optical glass flat that was cleaned in a solution of hot chromic-sulfuric acid, rinsed in distilled water, and blown dry. The measured reflectivity curve  $R(\alpha)$  is given in Fig. 3(a). For  $\alpha < \alpha_c$ , the reflectivity is close to 100%. A sharp drop in the reflected intensity is observed for  $\alpha \sim 0$  because the beam footprint exceeds the size of the sample at these small angles. Note that the reflectivity curve could be followed for seven orders of magnitude!

The reflectivity  $R(q)$  deviated from the Fresnel law as demonstrated in Fig. 3(b). The logarithm of  $R(q)/R_F(q)$  is linear in  $q^2$ . As discussed elsewhere, this indicates a surface with a mean square roughness amplitude  $\langle u^2 \rangle = 3.8 \pm 0.03$  Å, in very good agreement with both high-resolution synchrotron measurements<sup>30</sup> and with the mean square amplitude which is theoretically expected from thermally excited capillary waves.<sup>24,30,45,46</sup>

The liquid-crystal sample was a thin layer (0.5 mm) of 4-8-pentylphenyl 4-8-alkoxybenzoate ( $\bar{8}S5$ ) spread on a 51-mm-diam glass disk. The disk was placed inside a sealed cell, the temperature of which was controlled to  $\pm 1$  mK. The phase transition sequence of this sample is

Isotropic  $\xrightarrow{T_{NI} \sim 86^\circ\text{C}}$  Nematic  $\xrightarrow{T_{NA} \sim 63^\circ\text{C}}$  Smectic A  $\xrightarrow{T_{AC} \sim 58^\circ\text{C}}$  Smectic C  $\xrightarrow{T_M \sim 19^\circ\text{C}}$  Crystal.

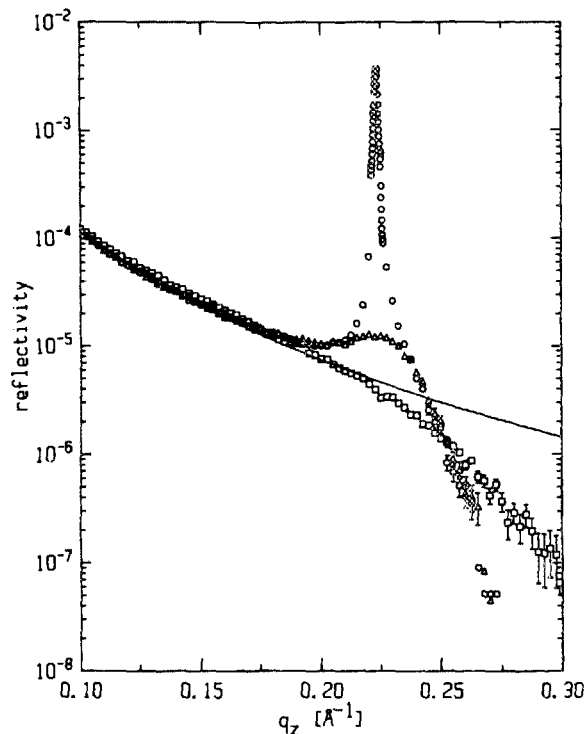


Fig. 4. X-ray reflectivity of the surface of the liquid crystal  $\bar{8}S5$ . The circles are for  $T = 60.673^\circ\text{C}$ , triangles for  $T = 69.578^\circ\text{C}$ , squares for  $T = 85.387^\circ\text{C}$ , and the solid line is the Fresnel law.

The measured surface reflectivity curves are given in Fig. 4 for a number of temperatures. In the nematic phase, the surface-induced smectic order, first observed by one of us (PSP) in octloxycyanobiphenyl (8OCB)<sup>22,29</sup> manifests itself as a peak at  $q_0 = 2\pi/D$ , where  $D = 28.24$  Å is the layer spacing in the bulk smectic phase. As the temperature is increased, the peak height decreases and its width increases, indicating a decrease of the correlation length of the thickness of the ordered layered region. Note that even well into the isotropic phase ( $T = 102^\circ\text{C}$ ), the surface still induces a small number of layers which is manifested in the sharp deviation of the reflectivity curve from the Fresnel law for  $q > q_0$ . A full study of this sample will be published elsewhere.<sup>47</sup>

## ACKNOWLEDGMENTS

We gratefully acknowledge the skilled assistance of Dan Schwartz in the measurements on the surface of water, the staff of the Scientific Instrument Shop in the Gordon McKay Laboratory in the construction of the spectrometer, and discussions with J. Als-Nielsen and S. A. Rice. This work was supported in part by the National Science Foundation through Grant No. NSF DMR 82-12189 and No. NSF DMR 83-16979 and by the Joint Services Electronics Program through Grant No. N00014-84-K-0465.

## APPENDIX A: FORMULAS FOR SETTING THE ANGLES OF INCIDENCE AND DETECTION

The angles  $\alpha$  and  $\beta$  (see Fig. 2) are established by setting the heights of elevators  $E_1 - E_4$ . These heights, denoted  $A_1 - A_4$ , are all measured relative to zero reference levels established during the lineup procedure, i.e., for horizontal setting ( $\alpha = \beta = 0$ )  $A_1 = A_2 = A_3 = A_4 = 0$  by definition. A negative sign denotes a downward displacement.

The relative parameters are  $H_1$ , the distance between the center of  $P_1$  and the center line of the x-ray beam;  $H_2$ , the displacement of the x-ray beam in the two-bounce crystal;  $L_1$ , the horizontal distance between the source spot and the pivot  $P_1$ ;  $L_3$ , the horizontal distance between the source spot and the center of the liquid surface;  $L_2$ , the horizontal distance between pivots  $P_1$  and  $P_2$ ;  $L_4$ , the horizontal distance between the center of the liquid surface and slit  $S_4$ ;  $A_1 - A_4$  are given in terms of  $\alpha$  and  $\beta$  by

$$A_1 = -L_1 \tan \alpha + H_1(1 - 1/\cos \alpha), \quad (\text{A1})$$

$$A_2 = A_1 - L_2 \tan \alpha, \quad (\text{A2})$$

$$A_3 = -L_3 \tan \alpha + H_2(1 - 1/\cos \alpha), \quad (\text{A3})$$

$$A_4 = A_3 + L_4 \tan \beta. \quad (\text{A4})$$

Equations used to calculate  $\alpha$  and  $\beta$  in terms of  $A_1 - A_4$ :

$$\alpha = \tan^{-1}[(A_1 - A_2)/L_2], \quad (\text{A5})$$

$$\beta = \tan^{-1}[(A_4 - A_3)/L_4]. \quad (\text{A6})$$

Note that negligible small terms arising from the unequal diameters of the pin and ball in  $P_1$  and  $P_2$  were omitted from the equations above.

## APPENDIX B: MOMENTUM-SPACE-REAL-SPACE RELATIONS

Assuming that the sample has an in-plane preferred orientation such as a crystallographic axis, we chose that direction as the  $x$  axis. The  $z$  axis is taken to be perpendicular to the liquid surface (see Fig. 2). Then

$$\mathbf{k}_i = k(\cos \alpha \sin \phi, \cos \alpha \cos \phi, -\sin \alpha), \quad (\text{B1})$$

$$\mathbf{k}_o = k[-\cos \beta \sin(2\theta + \phi), \cos \beta \cos(2\theta + \phi), \sin \beta], \quad (\text{B2})$$

where  $k = 2\pi/\lambda$ .

The momentum transfer  $\mathbf{q} = \mathbf{k}_o - \mathbf{k}_i$  is given by

$$\mathbf{q} = k[-\cos \alpha \sin \phi - \cos \beta \sin(2\theta + \phi), \cos \beta \cos(2\theta + \phi) - \cos \alpha \cos \phi, \sin \beta + \sin \alpha]. \quad (\text{B3})$$

Since there is no unique inversion formula, it is convenient to choose  $\phi = 0$  which yields

$$\mathbf{q} = k(-\cos \beta \sin 2\theta, \times \cos \beta \cos 2\theta - \cos \alpha, \sin \beta + \sin \alpha). \quad (\text{B4})$$

Equation (B4) can be inverted to give

$$\alpha = \cos^{-1}(\Delta/k), \quad (\text{B5})$$

$$\beta = \sin^{-1}(q_z/k - \sin \alpha), \quad (\text{B6})$$

$$2\theta = -\sin^{-1}(q_z/k \cos \beta), \quad (\text{B7})$$

where

$$\Delta = -b + (b^2 - 4ac)^{1/2}/2a, \quad (\text{B8})$$

and

$$a = 1 + (q_y/q_z), \quad (\text{B9})$$

$$b = q^2(q_y/q_z), \quad (\text{B10})$$

$$c = q^4/(2q_z)^2 - k^2. \quad (\text{B11})$$

Note that Eqs. (B5)–(B11) hold only for the special case where  $\phi = 0$ . For another important special case,  $\alpha = \beta$ , Eq. (B3) can be inverted to yield

$$\alpha = \beta = \sin^{-1}(q_z/2k), \quad (\text{B12})$$

$$\phi = \tan^{-1}(-q_y/q_x) + 2\theta/2, \quad (\text{B13})$$

$$2\theta = 2 \sin^{-1}[(q_x^2 + q_y^2)^{1/2}/2k \cos \alpha]. \quad (\text{B14})$$

## APPENDIX C: LINEUP PROCEDURE

This section is intended to provide the reader with the essential elements of the lineup procedure. The major alignment consideration is to define the incident x-ray beam to be parallel with the liquid surface, i.e., normal to the gravitational field. Using a bubble level, elevators  $E_1$  and  $E_2$  are adjusted such that  $S_1$  and  $S_2$  are at approximately the same height. With the monochromator removed and with both  $S_1$  and  $S_2$  set at 0.1 mm high, the elevators  $E_1$  and  $E_2$  are moved simultaneously using the beam monitor as the detector. This procedure defines the height of the x-ray spot and the effective source size. The tracking of the source can be tested by scanning either  $E_1$  or  $E_2$  at fixed  $\alpha$  and any deviations are used to redefine  $H_1$  and  $L_2$  in order to improve the tracking.

The double bounce Bonse-Hart monochromator is set to the Bragg angle using a scintillation detector. With  $S_1$  and  $S_2$  set at 0.1 mm high the copper  $K\alpha_1$  and  $K\alpha_2$  lines can be clearly separated. Slit  $S_3$  is adjusted to be only slightly larger than the beam size in order to reduce parasitic scattering. The  $\phi$ ,  $2\theta$  goniometer translation is adjusted such that the beam intercepts the rotational axis of the goniometer. The  $2\theta$  arm and elevator  $E_4$  are adjusted to be centered on the x-ray beam. Elevators  $E_1$  and  $E_2$  are returned to the level beam position and elevator  $E_3$  is raised so that the sample intercepts half of the beam. The coarse lineup is completed.

With the detector slit reasonably wide open, the sample tracking is checked by performing sample height scans at several incident angles observing the specularly reflected signal. Any deviations in the tracking are used to redefine the source to sample distance ( $L_3$ ) to better precision. If the center of the sample is equidistant to the source and slit  $S_4$  ( $L_3 = L_4$ ), then x rays at all incident angles will reflect to the same height of slit  $S_4$ . Any deviations in the reflected beam height at  $S_4$  for different incident angles are used to move the position of  $S_4$  (i.e.,  $L_4$ ) such that this criteria is satisfied. This procedure is most sensitive at the largest angles and with  $S_4$  set to be as small as the beam size.

The zero angle of the incident beam has only been defined coarsely and a finer adjustment involves using a liquid surface as a reference. The reflected beam and the direct beam will intercept  $S_4$  at different elevator heights ( $E_4$ ), where the difference is  $\Delta Z$  (see Fig. 5). If  $\Delta Z$  is nonzero, then the zero angle of the spectrometer is misaligned by an

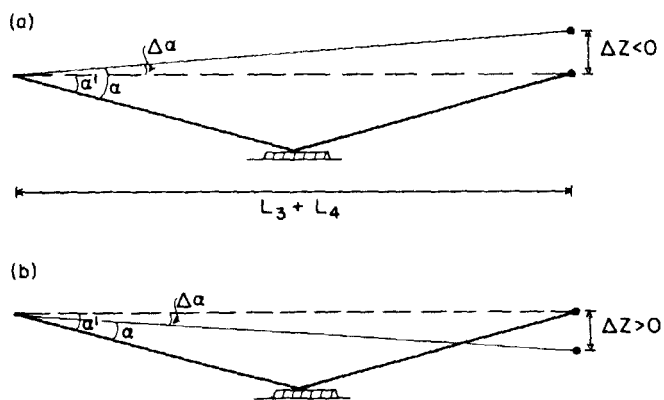


FIG. 5. Angular deviations for a misaligned spectrometer.

angle  $\Delta\alpha \approx \Delta Z / (L_3 + L_4)$ . By setting the spectrometer to  $\alpha = \Delta\alpha$  and with  $E_4$  at the position corresponding to the reflected beam, all of the elevators are reset to zero. If  $\Delta Z$  is large, it may be necessary to repeat this procedure several times. It is also a good idea to perform the other checks described previously.

The level of the beam cross section as it intercepts the sample surface is primarily defined by the tilt of slit  $S_2$ . With the present setup the only way to tilt  $S_2$  is by pivoting the entire mechanical beam via a tilt adjustment on pivot  $P_2$ . This also translates the x-ray beam laterally and the goniometer position must be reset. An improved design would allow a tilt of  $S_2$  on a Eulerian cradle. For either design, the slit is tilted such that the beam intercepts the sample at the same elevator height over the entire width of the beam.

<sup>a1</sup> Permanent address: Physics Department, University of Texas at Arlington, Arlington, Texas 76019.

<sup>b1</sup> Permanent address: Physics Department, Bar-Ilan University, Ramat-Gan, Israel.

<sup>1</sup> B. Widom, *Phase Transitions and Critical Phenomena* (Academic, New York, 1972).

<sup>2</sup> I. K. Robinson, *Phys. Rev. Lett.* **50**, 1145 (1983).

<sup>3</sup> M. P. D'Evelyn and S. A. Rice, *J. Chem. Phys.* **78**, 5225 (1983).

<sup>4</sup> M. P. D'Evelyn and S. A. Rice, *J. Chem. Phys.* **78**, 5081 (1983).

<sup>5</sup> K. K. Mon and D. Stroud, *Phys. Rev. Lett.* **45**, 817 (1980).

<sup>6</sup> S. Dietrick and H. Wagner, *Phys. Rev. Lett.* **51**, 1469 (1983).

<sup>7</sup> M. Robert, *Phys. Rev. Lett.* **54**, 444 (1985).

<sup>8</sup> J. Greyko and S. A. Rice, *J. Non-Cryst. Solids* **61&62**, 703 (1984).

<sup>9</sup> J. R. Eckardt, D. O. Edwards, S. Y. Shen, and F. M. Gasparini, *Phys. Rev. B* **16**, 1944 (1977).

<sup>10</sup> F. Watson, *Phys. Rev.* **12**, 257 (1901).

<sup>11</sup> F. Watson, *Phys. Rev.* **15**, 29 (1902).

<sup>12</sup> D. Langevin, *J. Phys. (Paris) Colloq. C-10*, **44**, 155, Paris (1983).

<sup>13</sup> Th. Rasing, Y. R. Shen, M. W. Kim, P. Valint Jr., and J. Bock, *Phys. Rev. A* **31**, 537 (1985).

<sup>14</sup> D. Beaglehole, *Phys. Rev. Lett.* **43**, 2016 (1979).

<sup>15</sup> D. Beaglehole, *J. Phys. (Paris) Colloq. C-10*, **44**, 147, Paris (1983).

<sup>16</sup> D. O. Edwards, *Physica* **109&110B**, 1531 (1982).

<sup>17</sup> L. J. Campbell, *Phys. Rev. B* **27**, 1913 (1983).

<sup>18</sup> J. H. Magerlein and T. M. Sanders, *Phys. Rev. Lett.* **56**, 258 (1976).

<sup>19</sup> J. Lekner and J. R. Henderson, *Physica* **94A**, 549 (1978).

<sup>20</sup> E. Brezin and S. Feng, *Phys. Rev. B* **29**, 472 (1984).

<sup>21</sup> P. S. Pershan, *J. Appl. Phys.* **45**, 1590 (1974).

<sup>22</sup> J. Als-Nielsen, F. Christensen, and P. S. Pershan, *Phys. Rev. Lett.* **48**, 1107 (1982).

<sup>23</sup> B. C. Lu and S. A. Rice, *J. Chem. Phys.* **68**, 5558 (1978).

<sup>24</sup> D. Sluis and S. A. Rice, *J. Chem. Phys.* **79**, 5658 (1983).

<sup>25</sup> D. Sluis, M. P. D'Evelyn, and S. A. Rice, *J. Chem. Phys.* **78**, 1611 (1983).

<sup>26</sup> L. Bosio, R. Cortes, A. Defrain, and M. Qumezine, *J. Non-Cryst. Solids* **61&63**, 699 (1984).

<sup>27</sup> L. Bosio and M. Qumezine, *J. Chem. Phys.* **80**, 959 (1984).

<sup>28</sup> J. Als-Nielsen and P. S. Pershan, *Nucl. Instrum. Methods* **208**, 545 (1983).

<sup>29</sup> P. S. Pershan and J. Als-Nielsen, *Phys. Rev. Lett.* **52**, 759 (1984).

<sup>30</sup> A. Braslau, M. Deutsch, P. S. Pershan, A. H. Weiss, and J. Als-Nielsen, *Phys. Rev. Lett.* **54**, 114 (1985).

<sup>31</sup> J. Als-Nielsen, A. Braslau, B. Ocko, and P. S. Pershan (to be published).

<sup>32</sup> P. Eisenberger and W. C. Marra, *Phys. Rev. Lett.* **46**, 1081 (1981).

<sup>33</sup> M. Seul, P. Eisenberger, and H. M. McConnell, *Proc. Natl. Acad. Sci. USA* **80**, 5795 (1983).

<sup>34</sup> J. M. Bloch, M. Sansone, F. Rondelez, D. G. Peiffer, P. Pincus, M. W. Kim and P. M. Eisenberger, *Phys. Rev. Lett.* **54**, 1039 (1985).

<sup>35</sup> R. S. Becker, J. A. Golovchenko, and J. R. Patel, *Phys. Rev. Lett.* **50**, 153 (1983).

<sup>36</sup> G. Vineyard, *Phys. Rev. B* **26**, 4146 (1982).

<sup>37</sup> Type 422, Huber Diffraction GmbH, Rimsting, West Germany.

<sup>38</sup> U. Bonse and M. Hart, *Appl. Phys. Lett.* **7**, 238 (1965).

<sup>39</sup> 50-mm translation stage, Aerotech Inc., Pittsburgh, PA.

<sup>40</sup> E. L. Church, H. A. Jenkinson, and J. M. Zavada, *Opt. Eng.* **18**, 125 (1979).

<sup>41</sup> R. W. James, in *The Optical Principles of the Diffraction of X-Rays*, edited by Sir Lawrence Bragg (Cornell University, Ithaca, NY 1965).

<sup>42</sup> L. G. Parratt, *Phys. Rev.* **95**, 359 (1954).

<sup>43</sup> P. Beckman and S. Spirizchino, in *The Scattering of Electromagnetic Waves from Rough Surfaces* (McMillan, New York, 1963).

<sup>44</sup> E. S. Wu and W. W. Webb, *Phys. Rev. A* **8**, 2065 (1973).

<sup>45</sup> F. P. Buff, R. A. Lovett, and F. H. Stillinger, *Phys. Rev. Lett.* **15**, 621 (1965).

<sup>46</sup> F. H. Stillinger, *J. Chem. Phys.* **76**, 1087 (1982).

<sup>47</sup> A. Braslau and P. S. Pershan (to be published).